J Mater Sci: Mater Med (2013) 24:863–876
DOI 10.1007/s10856-013-4871-z

Surface interactions of a W-DLC-coated biomedical AISI 316L stainless steel in physiological solution

Renato A. Antunes · Nelson Batista de Lima · Márcia de Almeida Rizzutto · Olga Zazuco Higa · Mitiko Saiki · Isolda Costa

Received: 15 September 2012 / Accepted: 18 January 2013 / Published online: 31 January 2013

Abstract The corrosion stability of a W-DLC coated surgical AISI 316L stainless steel in Hanks' solution has been evaluated. Particle induced X-ray emission (PIXE) measurements were performed to evaluate the incorporation of potentially bioactive elements from the physiological solution. The film structure was analyzed by X-ray diffractometry and micro-Raman spectroscopy. The wear behavior was assessed using the sphere-on-disc geometry. The in vitro biocompatibility of the W-DLC film was evaluated by cytotoxicity tests. The corrosion resistance of the stainless steel substrate decreased in the presence of the PVD layer. EIS measurements suggest that this behavior was closely related to the corrosion attack through the coating pores. PIXE measurements revealed the presence of Ca and P in the W-DLC film after immersion in Hanks' solution. This result shows that the PIXE technique can be applied to identify and evaluate the incorporation of bioactive elements by W-DLC films. The film showed good wear resistance and biocompatibility.

R. A. Antunes (✉)
Engineering, Modeling and Applied Social Sciences Center (CECS), Federal University of ABC (UFABC), Santo André, SP 09210-170, Brazil
e-mail: renato.antunes@ufabc.edu.br

N. B. de Lima · O. Z. Higa · M. Saiki · I. Costa
IPEN/CNEN-SP, Av. Prof. Lineu Prestes 2242, São Paulo, SP CEP 05508-900, Brazil

M. de Almeida Rizzutto
Nuclear Physics Department, Institute of Physics, University of São Paulo, IFUSP, São Paulo, Brazil

1 Introduction

The widespread use of metals for biomedical applications builds up the necessity of attaining critical performance targets involving fatigue, wear and corrosion behavior of materials without neglecting its biocompatibility [1–3]. These phenomena are often interconnected, making the development of high-performance biomaterials a challenging task for materials scientists. Corrosion resistance plays a central role in this scenario. Ion release from metallic implants can change the cellular metabolism, causing adverse biological reactions which can ultimately lead to failure of the implanted device [4]. Recently, Karimi et al. [5] reported that AISI 316L, Ti6Al4V and Co–28Cr–6Mo alloys released metallic ions when submitted to long-term corrosion experiments conducted in phosphate buffered solutions. Austenitic stainless steels are traditionally employed as load-bearing implant devices, either for temporary or permanent purposes. However, these materials are prone to corrosion upon contact with body fluids [6].

Intrinsically biocompatible ceramic hard coatings produced by physical vapor deposition (PVD) processes have emerged as potential candidates for the corrosion protection of metallic biomaterials for load-bearing applications. In addition to the anticorrosion properties these layers have also with attractive wear and fatigue resistance [7, 8]. TiN, TiCN and ZrN have been tested for the corrosion protection of biomedical metallic alloys [9–11]. Diamond-like carbon (DLC) films have been considered for the enhancement of the surface properties of orthopedic and cardiovascular devices [12, 13]. These films are typically amorphous, consisting of a network of sp^2 and sp^3 bonded carbon atoms. The ratio sp^3:sp^2 strongly affects the mechanical behavior of the DLC films. High sp^3:sp^2 ratios favor the formation of a hard

and brittle layer [14]. Moreover, this ratio also affects the adhesion of the coating to metallic substrates thereby influencing the corrosion barrier efficiency of the DLC layer [15]. DLC layers containing metals have been developed to increase adhesion to specific substrates [16]. Bewilogua et al. [17] produced Nb-DLC and Ti-DLC coatings by reactive dc magnetron sputtering. Wang et al. [18] deposited Cr-DLC and Zr-DLC films on titanium biomedical alloys. Baba and Hatada [19] developed tungsten-containing DLC (W-DLC) layers to improve the wear and adhesion properties of the original undoped DLC films. Other authors have also deposited W-DLC films on metallic substrates [20, 21]. Mansano et al. [22] showed that W-DLC coatings produced by reactive dc magnetron sputtering are highly biocompatible. Although the tribological properties of W-DLC films have received much attention, the study of the corrosion behavior of W-DLC coated metallic biomaterials has been neglected in the literature.

Proton induced X-ray emission (PIXE) is a non-destructive and high sensitivity physical method of multi-elemental quantitative analysis. The spatial resolution of the technique is 1 μm and the trace capability is in the order of ppm. Other analytical techniques for elemental analysis such as time of flight-secondary ion mass spectroscopy (TOF–SIMS) and Auger electron spectroscopy (AES) have typically better spatial resolution (15 nm for AES and 100 nm for TOF–SIMS) whereas the trace capability is 0.1 % for AES and sub-ppm for TOF–SIMS [23]. PIXE is considered the only analytical technique which is capable of determining the concentration of 20–30 elements in a non-destructive manner using a single and small sample ($\sim$5 mg) and with a very sensitive detection limit [24]. Moreover, the sample preparation is relatively simple and the analysis is fast [25]. Hence, it can be used as a first screening method to found potentially bioactive elements on the surface of implant materials. The method consists of irradiating the specimen to be analyzed with an ion beam (H^+, He^+), aiming the emission of characteristic X-ray whose energy is detected by a Si(Li) detector. The method is limited by the absorption in the detector window, identifying elements with atomic number $Z > 10$, being more sensitive in the ranges $20 < Z < 40$ and $Z > 70$. The method allows a chemical analysis with sensitivity of several ppm [26]. Owing to this powerful detection capability the technique is often employed to identify trace elements that contaminate tissues surrounding metallic prostheses [27, 28]. Other application in the biomedical field is the study of biomaterial/biological fluids interfaces, following the formation of calcium phosphate compounds on the surface of implanted biomaterials [29]. This approach is particularly frequent for the study of bioactivity in bioactive glasses [30, 31]. However, the use of PIXE to follow the incorporation of potentially bioactive elements in PVD films, and particularly in W-DLC films, has not been reported yet.

The aim of this work was to investigate the corrosion performance of a W-DLC coated AISI 316L biomedical alloy in Hanks' solution at 37 °C. Moreover, PIXE measurements were performed to evaluate the incorporation of Ca and P from the Hanks' solution in order to give an insight on the applicability of this technique to identify the presence of potentially bioactive elements on the surface of W-DLC films exposed to physiological media. The film structure was characterized by X-ray diffractometry and micro-Raman spectroscopy. The film morphology was observed by scanning electron microscopy. The wear behavior was assessed using the sphere-on-disc geometry. The in vitro biocompatibility was evaluated by cytotoxicity tests.

2 Experimental details

2.1 Substrate

The chemical composition of the medical grade AISI 316L stainless steel used in this work is given in Table 1.

2.2 W-DLC deposition

Initially the substrate was cleaned through an argon ion etching. DLC coating was deposited by means of a reactive dc magnetron sputtering method. The film consisted of a tungsten-containing DLC (W-DLC) with a thickness of $\sim$2 μm. The deposition system comprises a sputtering device with a pure tungsten target (99.99 % purity). The pressure of the process was kept constant at 0.8 Pa. The temperature of the substrate was held at 180 °C during deposition. The concentration of acetylene in the deposition chamber was 70 sccm and that of argon was 200 sccm.

2.3 Film structural characterization

The film structure was characterized by X-ray diffractometry using Cr Kα radiation using a Rigaku-Dmax 2000

Table 1 Chemical composition of the surgical 316L stainless steel

Element	C	Si	P	S	Cr	Mn	Cu	Ni	Mo	N	Fe
Mass (%)	0.01	0.37	0.01	0.002	17.4	1.78	0.03	13.5	2.12	0.07	Bal.

equipment. Micro-Raman spectroscopy was used to characterize the bonding structure of the W-DLC film with a 514 nm wavelength excitation source and Raman Renishaw instrument.

2.4 Scanning electron microscopy (SEM)

The morphology of the W-DLC film was observed through SEM analyses using a Philips XL30 microscope. Energy dispersive X-ray spectrometry (EDS) was used to test the elemental composition of the W-DLC film.

2.5 Electrochemical measurements

2.5.1 Film porosity

According to Ahn et al. [32] the corrosion resistance of a PVD-coated metallic substrate is limited by the intrinsic porosity of the film. Elsener et al. [33] proposed an electrochemical method to estimate the porosity of PVD layers based on the use of Eq. (1):

$$P = \left(\frac{R_{p,s}}{R_p}\right) \times 10^{-|\Delta E_{corr}|/b_a} \quad (1)$$

The porosity of the film is estimated from the change of the corrosion potential ($\Delta E_{corr} = E_{corr,substrate} - E_{corr,substrate+coating}$) caused by the presence of the coating layer and from individual measurements of the polarization resistance (R_p) of the bare and coated substrate. In Eq. (1) $R_{p,s}$ denotes the polarization resistance of the bare substrate and R_p is the polarization resistance of the coated substrate while b_a is the anodic Tafel slope of the bare substrate. $R_{p,s}$ b_a and are determined from separate measurements of the bare substrate. The values of R_p can be obtained by the linear polarization method which is valid only if the polarization current of the coating is negligible compared to that of the substrate and if the substrate does not passivated in the electrolyte [34]. Several authors employed this equation to estimate the porosity of PVD coatings [35, 36]. In this regard, the porosity of the W-DLC coating was determined using a SAE 1005 mild steel as substrate in a NaCl 0.5 M solution at room temperature. This condition does not induce any passivation in the mild steel. The W-DLC coating was produced according to the same processing parameters described in Sect. 2.2. The specimens were immersed for 1 h in the electrolyte to stabilize the corrosion potential. The measurements were performed using a potentiostat/galvanostat EG&G model 273A.

2.5.2 Electrochemical impedance spectroscopy (EIS)

The tests were performed at the open circuit potential, using a platinum wire as counter-electrode and a standard calomel electrode (SCE) as reference. The amplitude of the perturbation signal was 10 mV, the frequency range investigated was 100 kHz to 10 mHz with 6 points per decade using a frequency response analyzer (Solartron 1255) coupled to a potentiostat (EG&G 273A). The tests were performed at 37 °C in Hanks' solution. The composition of this solution is shown in Table 2. EIS plots were obtained after 1 and 28 days of immersion in the electrolyte. The results are given as Bode and Nyquist plots. The experimental data were fitted with equivalent circuits (ECs) using the Zview software to give a more quantitative analysis of the EIS response. The tests were conducted in triplicate to examine the reproducibility of the results. The data presented throughout this text are representative of the electrochemical behavior observed for each condition.

2.5.3 Potentiodynamic polarization curves

For the polarization measurements the experimental set-up comprised a three-electrode arrangement with a platinum wire and a saturated calomel electrode (SCE) as counter and reference electrodes, respectively. A potentiostat/galvanostat EG&G 273A was used for the measurements. Potentiodynamic polarization curves were obtained after 28 days of immersion in Hanks' solution at 37 °C for both bare and W-DLC-coated specimens, using a scanning rate of 1 mV s^{-1}. The potential range was from −0, 8 V_{ECS} to +1, 5 V_{ECS}. The tests were conducted in triplicate to examine the reproducibility of the results. The data presented throughout this text are representative of the electrochemical behavior observed for each condition.

2.6 Wear behavior

The wear resistance of uncoated and W-DLC coated AISI 316L specimens was evaluated using a Plint tribometer model TE66. The specimens were in the form of discs with 5 mm thickness and 100 mm diameter. The test is based on the sphere-on-disc geometry. The disc is fixed at the gyratory tribometer support. The sphere was a 6.35 mm silicon nitride ball which applied a 10 N load against the disc. The disc presented a 50 rpm rotation speed with a

Table 2 Chemical composition of Hanks' solution

Component	Concentration (M)
NaCl	0.1369
KCl	0.0054
$MgSO_4 \cdot 7H_2O$	0.0008
$CaCl_2 \cdot 2H_2O$	0.0013
$Na_2HPO_4 \cdot 2H_2O$	0.0003
KH_2PO_4	0.0004
$C_6H_{12}O_6 \cdot H_2O$	0.0050

radius of 25 mm. The total period of test was 30 min. After the tests, the discs have been observed in an optical microscope (Olympus) to evaluate the damages made by the sphere on their surfaces.

2.7 Particle induced X-ray emission (PIXE) measurements

Particle induced X-ray emission (PIXE) measurements were performed at the LAMFI (Laboratório de Análise de Materiais por Feixes Iônicos) at the University of São Paulo using a 2.4 MeV proton beam to generate characteristic X-rays of the samples. A detailed description of the PIXE measurement method is given elsewhere [37]. The analyses were conducted with the bare substrate and the W-DLC-coated stainless steel. The measurements were performed in triplicate, using specimens which were not immersed in physiological solution and with specimens immersed in Hanks' solution at 37 °C for 28 days.

2.8 Neutron activation analysis

Metal ions release from uncoated 316L and W-DLC coated 316L specimens was assessed using neutron activation analysis (NAA). The specimens were immersed for 28 days at 37 °C in Hanks' solution. After this period, NAA was used to determine the metallic elements in solution. The complete NAA procedure is described in detail elsewhere [38].

2.9 In vitro biocompatibility

The in vitro biocompatibity was performed with Chinese Hamster ovary cell line (CHO-k1). The cells were maintained in RPMI medium supplemented with antibiotics and antimicotic (100 units mL^{-1} penicillin, 100 μg mL^{-1} streptomycin and 0.025 μg mL^{-1} amphotericin), 2 mM glutamine, and 10 % fetal bovine serum, at 37 °C in a humidified 5 % CO_2 atmosphere until they reached confluence. For subculturing and for experiments, cells were harvested using 0.05 % trypsin and 0.02 % EDTA in phosphate-buffered solution, pH 7.4. Bare 316L and W-DLC coated 316L were sterilized by heating and immersed in RPMI medium, using the ratio between the surface area and the volume of extraction vehicle of 1 cm^2 mL^{-1} at 37 °C for 48 h. The extract was used to carry out the cytotoxicity test, according to ISO 10993 part 5 [39].

Cytotoxicity test was performed in 96 well microplates seeded with 3,000 cells per well and extracts dilutions from 100 to 6.25 %. The microplates were incubated for 72 h at 37 °C in a humidified 5 % CO_2 atmosphere. The cell viability was measured by adding 20 μL of MTS/PMS (20:1) solution and incubated for 2 h at 37 °C in the humidified 5 % CO_2 incubator. The microplates were read in a spectrophotometer reader at 495 nm. The test was compared with a negative control consisting of a titanium plate and a positive control of phenol 0.3 wt% in saline 0.9 wt% solution. The Index of Cytotoxicity for 50 % of cell viability (IC50) was estimated graphically.

3 Results and discussion

3.1 Film structural and morphological characterization

Figure 1 displays the XRD pattern of the W-DLC film. The film presents two broad peaks typical of amorphous carbon films. The asymmetry in the main broad peak was already observed and is associated with traces of crystallinity, suggesting the presence of carbide nanocrystals in the amorphous carbon matrix [21].

The Raman spectrum for the W-DLC film is shown in Fig. 2. The spectrum consists of a main G band at 1,545 cm^{-1} and a broad shoulder D band at 1,330 cm^{-1}. These broad peaks are typical of amorphous coatings. The most intense band arises from lattice vibration of sp^2-bonded carbon atoms (graphite or G band). The D peak is due to a disordered zone of graphite, leading to a lack of long-range order in the graphite sheets [40]. Disorder is frequently induced by grain boundaries or imperfections such sp^3-bonded carbon atoms or impurities [41].

As already mentioned in Sect. 1, DLC films have generally an amorphous nature and are comprised of a mixture of sp^3 and sp^2 bonded carbon atoms. The content of sp^3 bonds affects both the hardness and adhesion of DLC layers. Ferrari and Robertson [42] proposed a method to determine the sp^3 bond fraction in DLC films based on the experimental determination of the intensities of the G and D peaks obtained from Raman spectra and the position of the G peak. If the G peak is at 1,570 cm^{-1} the sp^3 content in the film is 10 %. If the G peak is around 1,550 cm^{-1} the sp^3 content is higher than 10 %. In

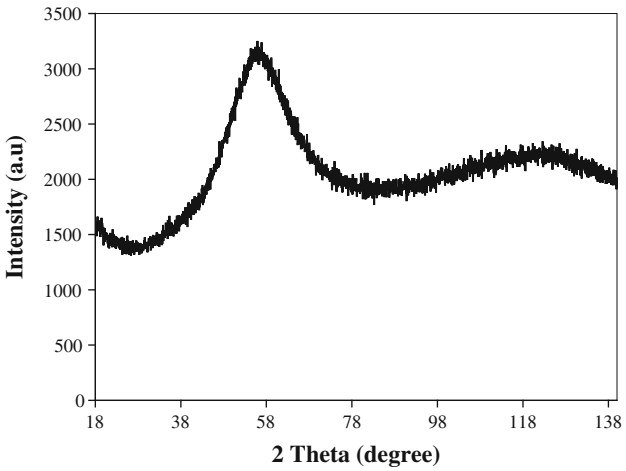

Fig. 1 XRD pattern of the W-DLC film

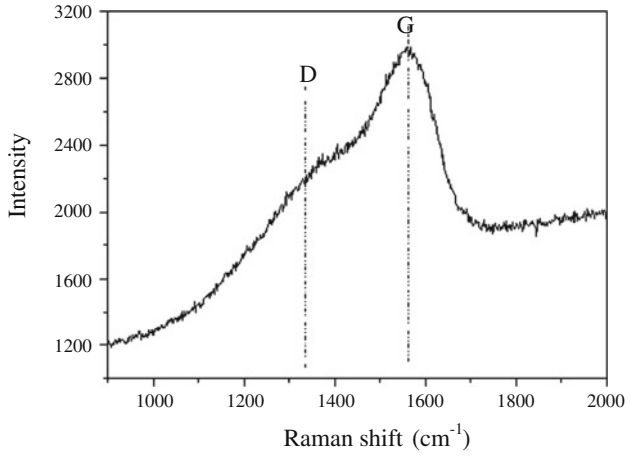

Fig. 2 Raman spectrum for the W-DLC film

this work the G peak occurs at 1,545 cm^{-1}, giving a I_D/I_G ratio of 0.67 and a sp^3 content of approximately 13 % according to the methodology of Robertson and Ferrari. Recently, Liu et al. [43] reported that a DLC film produced by plasma immersion ion implantation presented an I_D/I_G ratio of 0.65 showing excellent wear behavior. In this regard, our results agreed well with the literature.

The morphology of the W-DLC film was observed using SEM. The surface of the film is shown in Fig. 3a whereas its elemental composition is given in the EDS spectrum of Fig. 3b. The presence of tungsten is revealed.

Typical features of PVD coatings like pinholes and macroparticles are clearly seen on the specimen surface. These defects are intrinsic to PVD processes [44]. According to Panjan et al. [45] these defects are induced by surface irregularities such as pits, foreign particles (dust, debris) or during the deposition process (solidified droplets that stick on the substrate surface). The defects can act as preferential sites for the diffusion of aggressive ions present in the electrolyte in contact with the PVD-coated metal such as chlorides. This, in turn, can lead to localized corrosion attack. The electrochemical behavior of the W-DLC film is explored in the next section. Cross-sections of the coated substrate before immersion and after 28 days of immersion in Hanks' solution at 37 °C were also obtained as shown in the micrographs presented in Fig. 4. The aim of this analysis was to reveal possible visual effects of the immersion time on the morphology of the W-DLC layer. However, as seen in Fig. 4, it was not possible to identify significant differences in the compactness or thickness of the film before and after immersion.

3.2 Electrochemical tests

3.2.1 Film porosity

The results obtained from the linear polarization measurements of the bare and the W-DLC coated steel are

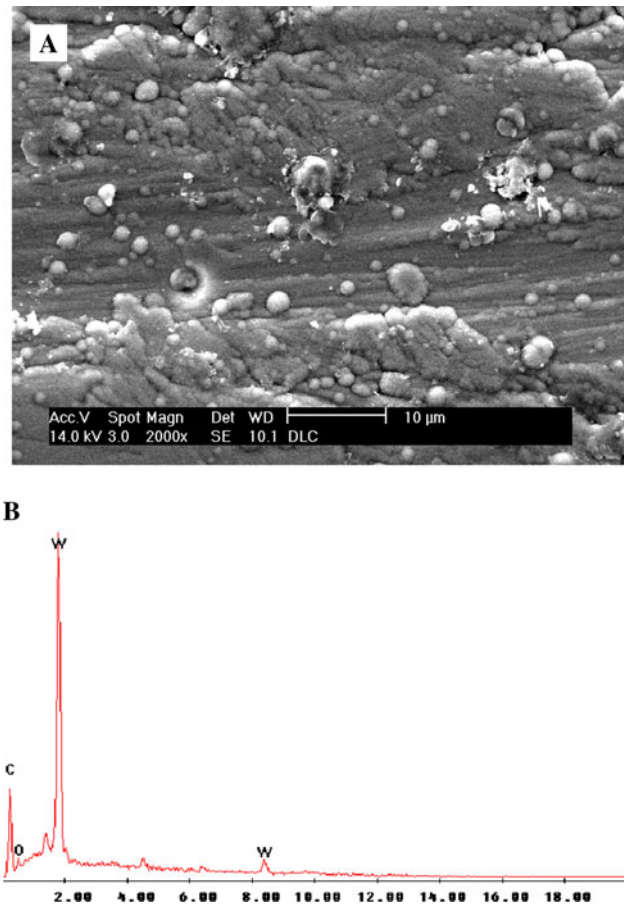

Fig. 3 **a** SEM micrograph showing the surface morphology; **b** EDS spectrum of the W-DLC film

shown in Table 3. The porosity of the film was calculated according to Eq. (1).

As seen in Fig. 3, the W-DLC layer is not defect-free. The result shown in Table 3 reveals that the film has an intrinsic porosity of 0.41 %. Porosity is a common characteristic of ceramic thin films produced by vapor deposition methods. Kim et al. [46] evaluated the porosity of DLC films produced by a chemical vapor deposition method using the linear polarization method. They found that the porosity of the DLC films was between 1.39 and 1.89 % depending on the voltage applied to the substrate during the deposition process. Choi et al. [47] determined the porosity of DLC films produced by chemical vapor deposition using the linear polarization method. The film presented a porosity of 3.01 %.

Depending on the deposition method and parameters, variable results can be found in the literature for different coating materials. Chenglong et al. [48] reported that a TiN coating deposited by arc ion plating on a surgical AISI 316L substrate presented a porosity of 3.74 % according to the linear polarization method. Merl et al. [36] used the

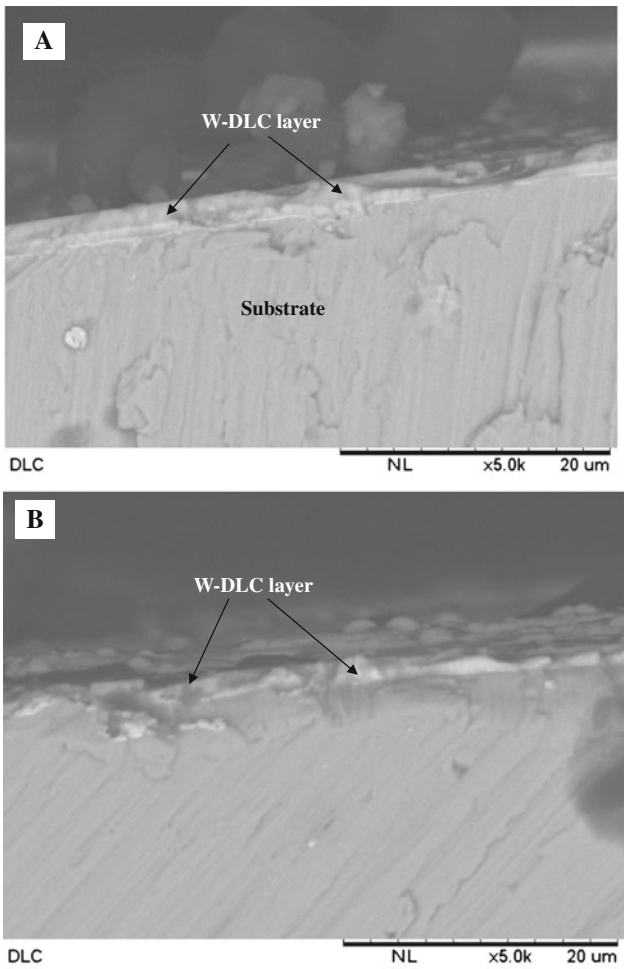

Fig. 4 Cross-sectional micrographs of the DLC layer: **a** before immersion and **b** after 28 days of immersion in Hanks' solution at 37 °C

same method to determine the porosity of CrN and Cr(C, N) coatings produced by arc ion plating on mild steel substrates. The porosity of the CrN film was 0.0028 % whereas that of the Cr(C, N) layer was 0.32 %. In this context, the most important reasoning derived from the porosity determination conducted in this work is to realize that the porosity level of the W-DLC film is relatively small. However, the defects present in the coating can act as potential sites for the onset of corrosion processes at the coating/substrate interface. This subject is investigated in the next two sub-sections.

3.2.2 *EIS measurements*

Bode plots of the bare AISI 316L and W-DLC-coated 316L specimens after different periods of immersion in Hanks' solution at 37 °C are shown in Fig. 5. The phase shift versus frequency plots show that bare 316L was highly capacitive after 1 day of immersion. This behavior is typical of passive metals and has been identified by other authors for 316L stainless steel [49]. The shape of the phase shift versus frequency plot was little altered with the immersion time. After 28 days the bare substrate still presented phase angles close to −80°, denoting the capacitive behavior of the passive film. Two time constants could be distinguished. The first one, characterized by a shoulder in the frequency range 10^2–10^3 Hz, can be related to the electrochemical response of the passive layer on the 316L surface. Considering that this oxide film has intrinsic defects that may facilitate the penetration of the electrolyte the physical meaning of the second time constant at lower frequencies can be interpreted as the response of the metallic substrate on the base of these defects. It is important to emphasize the stable character of the 316L substrate during the whole period of immersion which indicates its high corrosion resistance. This is also confirmed by the impedance values observed in the log |Z| versus frequency plots. There is a linear relationship between log |Z| and log f, with a slope close to −1 from the medium to the low frequency domains of the plots which is typical of a capacitive response. Furthermore, the impedance modulus was above 10^5 Ω cm^2 for all periods of immersion, denoting the protective nature of the passive film [50].

The phase shift versus frequency plots for the W-DLC-coated material presents a plateau at −70° for the phase angles from the medium to the low frequency domain for the initial periods of immersion (1 and 7 days). The evolution of the electrochemical behavior with time is clearly seen after 14 and 21 days of immersion. There was a decrease of the capacitive behavior of the coated-alloy and the development of a new time constant is apparent. The impedance values are not as stable as those of the 316L substrate as observed in the log |Z| versus log f plots which show a clear decrease from after 14 days of immersion. Furthermore, it is noticeable that the impedance values are always lower for the W-DLC coated 316L when compared with the uncoated alloy.

Table 3 Electrochemical parameters obtained from the linear polarization measurements and the calculated porosity of the W-DLC coating

$E_{corr,substrate}$ (mV)	$E_{corr,substrate+coating}$ (mV)	$R_{p,s}$ (Ω cm^2)	R_p (Ω cm^2)	b_a (mV/decade)	Porosity (%)
−741.2	−577	2,382	6,871	85	0.41

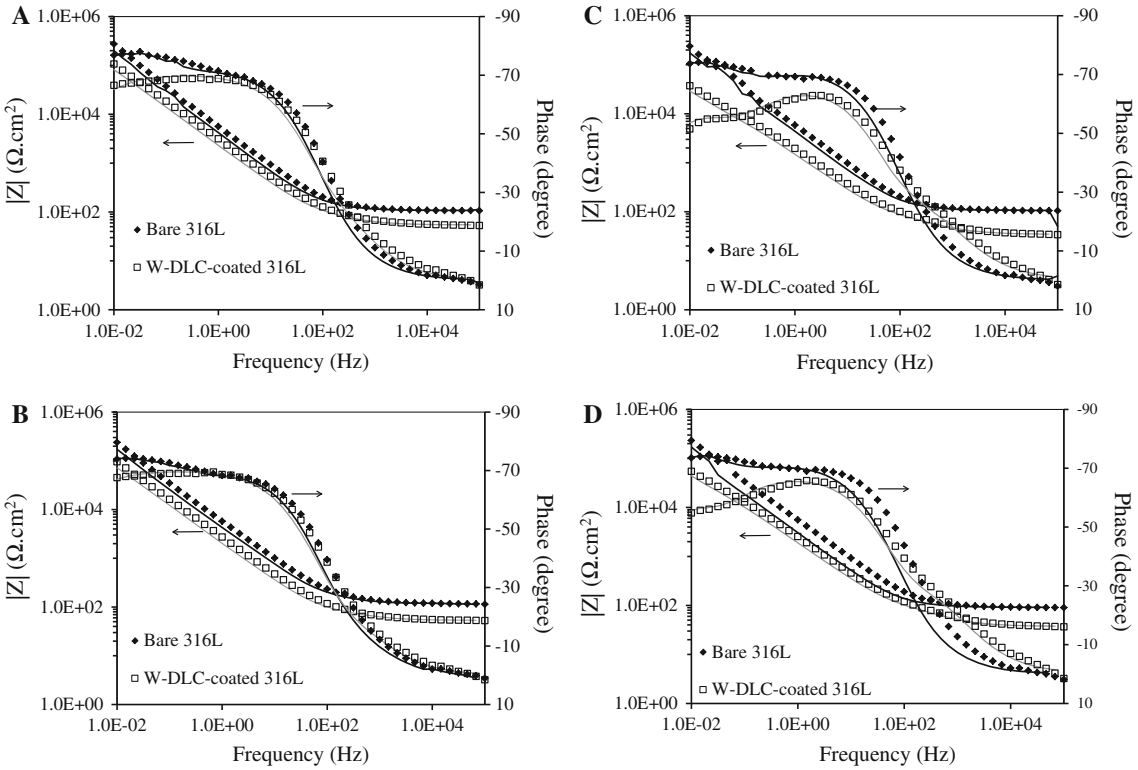

Fig. 5 *Plots* of the bare AISI 316L and W-DLC-coated 316L specimens after different periods of immersion in Hanks' solution at 37 °C: **a** 1 day; **b** 7 days; **c** 14 days; **d** 21 days

In order to give a further insight into this subject and a more quantitative analysis of the EIS response, the experimental data were fitted using equivalent electrical circuits (EECs) through a non-linear least square (NLLS) fitting procedure. The capacitive behavior was simulated using constant phase elements (CPEs) instead of pure capacitors accounting for the inhomogeneity of the materials surfaces. The parameters obtained from the modeling of the EIS data as a function of the immersion time are summarized in Table 4 for the uncoated substrate and in Table 5 for the W-DLC-coated 316L. Q and n are the magnitude and the exponent of the constant phase element (CPE), respectively. The CPE impedance (Z_{CPE}) is described by Eq. (2) [51]. Q is identified with the capacitance of the CPE [52], jω is the complex variable for sinusoidal perturbations and n varies between −1 and 1. The value of n is associated with the non-uniform distribution of current due to roughness and surface defects [53]. The EIS response depended on the immersion time and on the presence of the W-DLC film. Consequently, three different EECs were employed to simulate the experimental data. These EECs are shown in Fig. 6. The fitted data appears as solid lines in Fig. 5.

$$Z_{CPE} = [Q(j\omega)^n]^{-1} \quad (2)$$

The experimental data of bare 316L were fitted using the EEC shown in Fig. 6a. This circuit was used by Zou et al. [54] to model the EIS response of a 316L surgical stainless steel in Tyrode's simulated body fluid at 37 °C. Kocijan et al. [55] have also employed this EEC to simulate the EIS experimental results of a 316L stainless steel in artificial saliva. The physical meaning of the elements in this EEC can be given as follows: R_1 is the electrolyte resistance; CPE_1 represents the capacitive behavior of the passive film formed on the surface of the 316L stainless steel and R2 the electrical resistance of the film defects to the penetration of the electrolyte; CPE_2 is associated with the double layer capacitance whereas R3 is related to the charge transfer resistance. The results of the fitting procedure are summarized in Table 4. From Table 4 it is seen that R_2 increases with the immersion time and Q_1 (the capacitance of

Table 4 Equivalent circuit parameters obtained by fitting the electrochemical impedance data for AISI 316L substrate

Element	Bare 316L			
	1 day	7 days	14 days	21 days
R_1 (Ω cm^2)	112	122	94.6	101
Q_1 (10^{-5} cm^{-2} s^{-n} Ω)	2.82	3.02	3.19	3.25
n_1	0.87	0.84	0.85	0.84
R_2 (Ω cm^2)	10,950	16,358	23,148	26,132
Q_2 (10^{-5} cm^{-2} s^{-n} Ω)	1.17	1.28	1.30	1.33
n_2	0.97	0.94	0.94	0.93
R_3 (kΩ cm^2)	1,972	1,648	1,527	1,332

Table 5 Equivalent circuit parameters obtained by fitting the electrochemical impedance data for W-DLC coated 316L

Element	W-DLC coated 316L			
	1 day	7 days	14 days	21 days
R_1 (Ω cm^2)	54	53	49	50
Q_1 (10^{-4} cm^{-2} s^{-n} Ω)	0.51	0.35	0.47	0.73
n_1	0.77	0.80	0.75	0.72
R_2 (Ω cm^2)	114	88	96	90
Q_2 (10^{-4} cm^{-2} s^{-n} Ω)	0.26	0.53	0.93	0.97
n_2	0.81	0.77	0.89	0.76
R_3 (kΩ cm^2)	813	1,180	175	138
Q_3 (10^{-4} cm^{-2} s^{-n} Ω)	–	–	0.50	0.51
n_3	–	–	0.78	0.80
R_4 (kΩ cm^2)	–	–	60	21

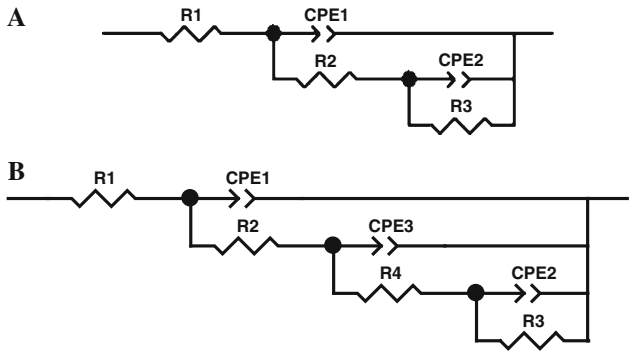

Fig. 6 Equivalent circuits used for fitting EIS data of **a** AIS 316L substrate and W-DLC-coated 316L after 1 and 7 days of immersion in the electrolyte; **b** W-DLC-coated 316L after 14 and 21 days of immersion in the electrolyte

the CPE_1 element) slightly increases. During the initial period of immersion the electrolyte penetrates through the defects of the passive film. For longer immersion times, this film becomes progressively thicker. Thus, the thickening of the outer layer would reflect in an increase of its capacitance Q_1 and an increase of its resistance R_2. According to the literature [56], an increase of the resistance and a reduction of the capacitance would indicate the formation of a less defective oxide layer with the immersion time. The evolution of R_3 and Q_2 with time is opposite to this tendency, suggesting that the charge transfer reactions are enhanced with time. The penetration of chloride ions present in the electrolyte through the passive film defects could account for this detrimental effect. These ions would reach the interface passive film/metallic substrate, accelerating the charge transfer reactions. This, in turn, would lead to the decrease of the resistance R_3 and the increase of the capacitance Q_2.

The EIS response of W-DLC-coated 316L was fitted using different models. The EEC shown in Fig. 6a gave the best fitting for 1 and 7 days of immersion. This circuit is often used to simulate the experimental data of coated metals when the coating presents defects such as pores and pinholes. Several authors have successfully employed this circuit to fit the EIS data of PVD-coated metals [57–59]. Kim et al. [46] used this EEC to simulate the EIS response of a DLC-Ti–6Al–4V alloy immersed in NaCl solution at 37 °C for 9 days. The model consists of the electrolyte resistance (R_1) in series with two elements R-CPE. The first time constant models the W-DLC film response consisting of the pore resistance (R_2) which results from the formation of ionic conduction paths across the coating thickness and the associated capacitance of the CPE (Q_1). The second time constant models the EIS response of the substrate in the base of the coating defects consisting of the charge transfer resistance (R_3) and the double layer capacitance (Q_2). After 14 days of immersion the quality of the fitting procedure was significantly reduced when this model was used. Thus, the circuit of Fig. 6a was modified by the introduction of a new time constant at the intermediate frequency domain as shown in Fig. 6b. This model gave the best fitting to the experimental data obtained after 14 and 21 days of immersion. R_1, Q_1, R_2, Q_2 and R_3 have the same physical meaning described for the model shown in Fig. 6a. The intermediate time constant consisting of the Q_3 and R_4 elements was introduced to model the response of corrosion products at the base of the coating defects. The formation of such products is likely to occur as a result of the charge transfer reactions at the interface between the electrolyte and the metallic substrate at the base of the film defects. The intrinsic porosity of the PVD layer is probably increased with the immersion time, facilitating the penetration of the electrolyte. This behavior has been observed for CrN layers produced by PVD processes [36]. This, in turn, would give rise to an acceleration of the corrosion processes at the base of the film defects, allowing the formation of an oxide layer with an incipient anticorrosion character. The relatively low values of R_4 in comparison with the charge transfer resistance values (R_3) confirm this assumption. In this regard, a new time constant developed in the system after 14 days of immersion which was modeled by the resistance of the corrosion products R_4 and its capacitance Q_3. The evolution of the EIS response shows that the charge transfer resistance (R_3) sharply decreased for the W-DLC-coated specimen as shown in Table 5. This analysis reveals that EIS is a powerful tool to study the evolution of the electrochemical behavior of PVD films. If on one hand it is difficult to assess morphological alterations of the W-DLC layer with the immersion time through SEM cross-sectional views (Fig. 4), on the other hand EIS gives irrefutable indications of the progress of electrochemical parameters of the film. This evolution, in turn, is closely related to the film morphology.

3.2.3 Potentiodynamic polarization curves

Potentiodynamic polarization curves of the bare AISI 316L and W-DLC-coated 316L specimens obtained after 28 days of immersion in Hanks' solution at 37 °C are shown in Fig. 7. The corrosion potential (E_{corr}) was only slightly affected by the W-DLC layer, being −0.32 V for the bare 316L and −0.33 V for the W-DLC-coated material. However, the corrosion current density (i_{corr}) of the coated alloy, determined from the extrapolation of the cathodic branch of the polarization curve up to the corrosion potential, was one order of magnitude higher that that of the uncoated 316L (3.56 μA cm^{-2} for the coated and 0.18 μA cm^{-2} for the uncoated material).

There is a passive region in the anodic branch of the curve obtained for the uncoated 316L ranging from −0.20 V up to breakdown potential (E_b) at +0.39 V. At this point the current density sharply increased, suggesting the onset of pitting corrosion. The anodic branch of the polarization curve obtained for the W-DLC-coated material presents a different behavior. The current density presents a slow and continuous increase with the corrosion potential. This behavior resembles that of active materials. Moreover, the anodic currents are higher than those observed for the uncoated 316L up to the point where the breakdown potential was reached. Several authors reported that DLC films act as effective anticorrosion barriers to metallic substrates [60, 61]. Nevertheless, Mohan et al. [62] reported that a DLC film had only a marginal effect on the corrosion resistance of a Ti–Mo alloy. Some authors have found that the presence of PVD layers can even degrade the corrosion properties of metallic substrates [63]. Coating morphology is the key factor that leads to a desirable corrosion resistance improvement or a deleterious poorly protective character. The potentiodynamic curves of Fig. 7 show that the W-DLC film did not provide a suitable protection to the 316L substrate. This finding corroborates EIS results. The incipient protective character imparted by the PVD layer is directly related to the presence of permeable defects in the film. However, the W-DLC film does have a positive effect on the pitting corrosion resistance in comparison with the bare material. Corrosion resistance allied with the well-known ability of DLC films to improve the tribological properties of metallic substrates [16] is important for biomedical applications. The proper control of deposition parameters such as substrate bias, temperature and current density could lead to the formation of a more compact, denser and corrosion resistant PVD layer [64].

3.3 Wear behavior

The variation of the coefficient of friction of uncoated and W-DLC-coated 316L specimens with the sliding distance is shown in Fig. 8. It is worth noting that uncoated 316L presented a continuous increase of the coefficient of friction. The test was prematurely interrupted when the sliding distance reached 6 m which was equivalent to a period of 2 min. This interruption was intentionally done due to an excessive vibration of the test device during the experiment. The vibration was originated from the intense friction between the silicon nitride sphere and the uncoated 316L disc. For the W-DLC-coated 316L the variation of the coefficient was much softer and the experiment was not interrupted, reaching a sliding distance of 289 m after 30 min.

After the sphere-on-disc tests the surface of each disc was observed using an optical microscope. The wear track of the W-DLC-coated disc presented fewer signs of degradation when compared to uncoated 316L disc. Optical micrographs of uncoated and W-DLC-coated 316L discs obtained after the sphere-on-disc tests are shown in Fig. 9. As clearly seen, the uncoated 316L disc presented is much more prone to wear than the PVD-coated disc. The

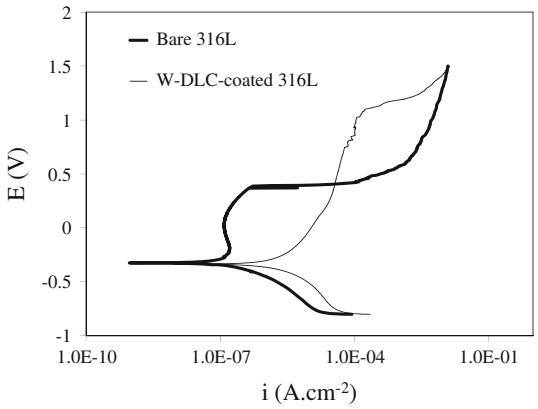

Fig. 7 Potentiodynamic polarization *curves* of bare and W-DLC-coated 316L obtained after 28 days of immersion in Hanks' solution at 37 °C

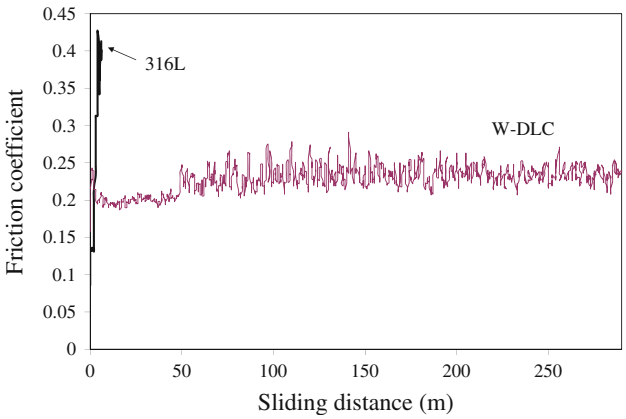

Fig. 8 Friction coefficient of uncoated and W-DLC-coated 316L discs

degradation observed in the wear track of this material after the test was significantly more intense when compared to the W-DLC-coated disc. So, it is clear that W-DLC film evaluated in this work was efficient at increasing the wear resistance of the 316L stainless steel. This is an essential property for implant devices.

3.4 PIXE measurements

The PIXE results for the concentration of elements on the surface of the uncoated AISI 316L stainless steel non-immersed and immersed in Hanks' solution at 37 °C for 28 days are shown in Table 6. Only the main alloying elements of the steel (Fe, Cr, Ni and Mo) and the potentially bioactive elements (Ca and P) are displayed in the table. The data are referred to the mean values of three different samples tested under the same conditions.

Phosphorus was not detected in the non-immersed specimen. After immersion the phosphorus concentration was 0.09 %. Calcium, in turn, was detected as an impurity in the non-immersed specimen. After immersion, its concentration presented a twofold increase. Egeni et al. [65] showed that PIXE was capable of detecting deposits of calcium and phosphorus ions on titanium implants tested under in vivo conditions. Our results point to a high sensitivity of the PIXE technique, allowing the determination of very few amounts of potentially bioactive elements after immersion in the physiological solution. It is important to emphasize, though, that this does not indicate a bioactive response of the stainless steel surface. This result should be rather considered as an evidence of the sensitivity of the PIXE technique which makes it suitable for investigating interfaces between tissues and implants. Moreover, it is interesting to note that the concentrations of the major alloying elements (Fe, Ni, Mo and Cr) did not decrease after immersion. This suggests that these elements have been not released to the physiological solution at significant amounts, thus pointing to a relative stability of the passive film under the testing conditions.

Table 7 shows the PIXE results for the concentration of elements on the surface of the W-DLC-coated stainless steel non-immersed and immersed in Hanks' solution at 37 °C for 28 days. Only the main alloying elements of the steel (Fe, Cr, Ni and Mo), the potentially bioactive elements (Ca and P) and the main constituent of the film (W for the W-DLC film) are displayed in the table. Carbon is not displayed due to the limitation of PIXE to detect elements with $Z < 15$. It is clear that for the W-DLC-coated steel the amount of Ca increased more significantly after immersion in Hanks' solution. The phosphorus content, in turn, was only slightly higher after immersion. As mentioned for the uncoated substrate, this result cannot be interpreted as an irrefutable evidence of the formation of bioactive compounds on the surface of the W-DLC film as PIXE only identifies each element separately. The PIXE method has intrinsic uncertainties associated with the relative small peak area of the light elements such as P. The uncertainties are indicated in the captions of Tables 6 and 7. In spite of this intrinsic experimental error, it

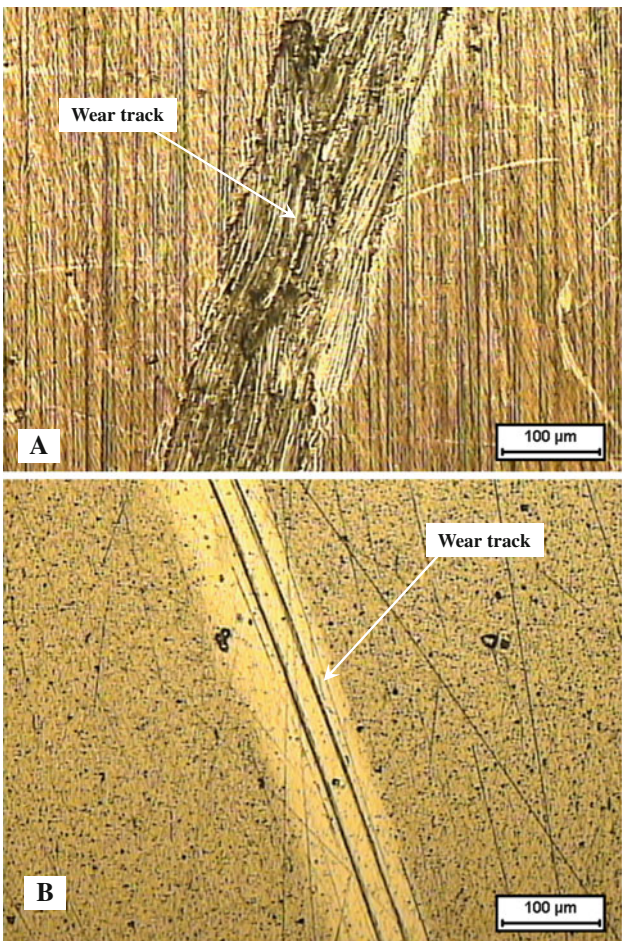

Fig. 9 Optical micrographs of the: **a** uncoated and **b** W-DLC-coated 316L discs after the sphere-on-disc wear test

Table 6 PIXE results for the concentration of elements on the surface of the uncoated AISI 316L stainless steel non-immersed and immersed in Hanks' solution at 37 °C for 28 days (uncertain values are ~10 % for P and Ca and 3 % for others elements)

	Concentration (mass %)	
Element	Non-immersed	Immersed
P	–	0.09 ± 0.04
Ca	0.02 ± 0.00	0.04 ± 0.02
Fe	60.7 ± 0.21	60.5 ± 0.21
Cr	21.0 ± 0.00	20.9 ± 0.17
Ni	13.2 ± 0.07	13.2 ± 0.17
Mo	1.86 ± 0.00	1.95 ± 0.03

The data are referred to the mean values of three different samples tested under the same conditions

is possible to affirm that the calcium content found in W-DLC-coated samples after immersion is statistically significant. The high standard deviation indicates that the results are asymmetric for this element. This implies that the incorporation of calcium is a phenomenon that was not homogeneous for all samples analyzed by PIXE. This is an expected result, as the intrinsic defects on the coating layer will probably give rise to different degrees of porosity during the immersion time and, thus, to different interactions with the elements present in the physiological solution. The same occurs for the phosphorus content of the uncoated stainless steel, as can be seen in Table 6. Thus, the prominent increase of the calcium concentration is a strong indication the W-DLC film has the ability to incorporate elements from the physiological solution. Another indication toward this direction is that potassium, which is also present in Hanks' solution, was also identified after immersion. This element was not found on the uncoated stainless steel substrate after immersion, suggesting that the intrinsic porosity of the W-DLC layer contributes to the incorporation of elements from the solution.

Several authors have investigated the osteoinductive behavior of diamond like carbon films [66, 67]. Olivares et al. [66] showed that amorphous carbon coatings deposited on 316L stainless steel samples by a PVD method promoted cell differentiation, leading to the formation of mineralized bone-like nodules. Some degree of porosity has been reported to favor the osseointegration process of implant surfaces [68]. Thus, it is likely that the presence of a relatively porous surface film could facilitate the incorporation of bioactive elements. The W-DLC film tested in this work has intrinsic defects and porosity that could act as preferential sites for this process. PIXE analysis provided a strong indication that phosphorus and, especially, calcium have been incorporated into the W-DLC layer.

Table 7 PIXE results for the concentration of elements on the surface of the DLC film non-immersed and immersed in Hanks' solution at 37 °C for 28 days (uncertain values are ~10 % for P and Ca and 3 % for others elements)

	Concentration (mass %)	
Element	Non-immersed	Immersed
P	0.12 ± 0.01	0.14 ± 0.01
K	–	0.07 ± 0.01
Ca	0.01 ± 0.00	0.11 ± 0.13
Fe	54.1 ± 1.21	52.7 ± 0.14
Cr	18.2 ± 0.35	17.8 ± 0.07
Ni	10.4 ± 2.09	11.5 ± 0.14
Mo	1.42 ± 0.17	1.39 ± 0.13
W	5.59 ± 0.32	5.81 ± 0.04

The data are referred to the mean values of three different samples tested under the same conditions

3.5 Neutron activation analysis (NAA)

The results obtained by NAA are shown in Table 8. Only the main alloying elements of the 316L stainless steel substrate were analyzed, that is, Fe, Cr, Ni and Mo. For the W-DLC-coated material tungsten was also analyzed. The numbers shown in Table 8 are referred to the detection limits of the NAA. None of the elements have been found in concentrations above the detection limit. This is an indication that the W-DLC layer and the passive film on the uncoated 316L were stable under the testing conditions. However, it should not be disregarded that the elements could be present in quantities below the detection limit of the NAA technique. This result suggests that, in spite of the porosity of the W-DLC film, the amount of metallic ions released to the physiological was small.

3.6 Cytotoxicity test

Cytotoxicity tests of uncoated and W-DLC-coated 316L were carried out by a colorimetric method based on the quantitative assessment of surviving viable cells upon exposure to the toxic agent. The amount of MTS, the marker of cell viability, taken up by the population of cells, is directly proportional to the number of viable cells in the culture [69]. The results are shown in Fig. 10 as a plot of the cell viability versus the extract concentration. Both the uncoated and W-DLC-coated 316L were not cytotoxic showing their harmless character. To confirm the reliability of the method the positive control showed a cytotoxic effect over the cells ($IC_{50} = 15$). This is a primary indication of the suitability of the W-DLC-coated 316L stainless steel for biomedical applications. Salgueiredo et al. [70] reported that conventional DLC coatings produced by DC magnetron sputtering presented no evidence of cytotoxicity upon contact with MG63 osteoblast-like cells. Sui et al. [71] showed that the blood compatibility of a NiTi alloy was improved by DLC films produced by plasma immersion ion implantation and deposition (PIIID). Bendavid et al. [72] reported good biocompatibility for DLC and DLC-Si films produced by a chemical vapor deposition process. In the case of W-DLC films the effect of tungsten

Table 8 Detection limits of the elements as obtained by NAA

Element (μg mL^{-1})	W-DLC	316L
Cr	<4.8	<4.0
Fe	<0.3	<5.6
Mo	<0.05	<0.15
Ni	<0.2	<2.5
W	<1.1	–[a]

[a] The detection limit was not determined

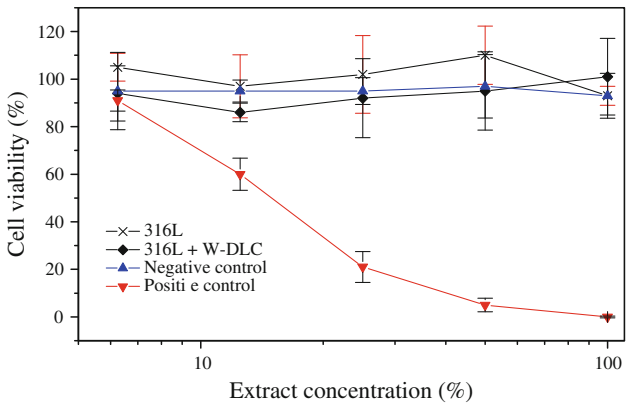

Fig. 10 Cell viability *curves* of the uncoated and W-DLC-coated 316L stainless steel

has to be taken into account. Mansano et al. [22] have confirmed the non-toxic character of W-DLC films. However, Witten et al. [73] reviews a series of papers which indicate that tungsten alloys have potential action in the development of tumors. Yet, the concentration of tungsten which comprises a risk to the health of human beings is not known. The authors state that this area needs additional research. According to the results reported here and those by Mansano et al. [22] W-DLC films did no present cytotoxicity. A complete evaluation involving in vivo tests is demanded for future work.

4 Conclusions

The corrosion stability of W-DLC-coated 316L specimens has been evaluated. The film morphology was observed through SEM micrographs, revealing the presence of intrinsic defects formed during the deposition process. These defects had a marked influence on the electrochemical behavior of the coated material. The porosity of the film was determined by means of the linear polarization method, indicating that the W-DLC layer presented an intrinsic porosity of 0.41 %. Electrochemical impedance measurements proved to be sensitive to this porosity level. The decrease of the charge transfer resistance of the coated material with the immersion time is a clear effect of the penetration of the electrolyte through the coating pores. Moreover, the results suggest that the porosity level increase with time, giving rise to a new time constant in the system. The potentiodynamic polarization curves confirmed the EIS results, evidencing the reduction of corrosion resistance of the W-DLC-coated 316L in comparison with the bare substrate. PIXE proved to be a valuable tool to detect the presence of potentially bioactive elements on the surface of PVD films. The porosity of the W-DLC layers seems to be important to facilitate the incorporation of Ca and P from the physiological solution. The suitability of W-DLC film for biomedical applications was confirmed by wear tests and in vitro biocompatibility assessment.

Acknowledgments The authors are thankful to Bodycote Brasimet S. A., especially to Dr. Ronaldo Ruas for the deposition of W-DLC films and to CNPq (National Council of Scientific and Technological Development) for the financial support to this work. Dr. Dalva L. A. de Faria from the University of São Paulo (IQUSP) is kindly acknowledged for her invaluable assistance with the Raman spectroscopy measurements. Mr. Celso V. de Morais (IPEN/CNEN) is acknowledged for the use of the scanning electron microscope. Mr. Leandro Justino de Paula from the University of São Paulo (Surface Phenomena Laboratory) is acknowledged for the assistance with the wear tests.

References

1. Gu XN, Zhou WR, Zheng YF, Cheng Y, Wei SC, Zhong SP, Xi TF, Chen LJ. Corrosion fatigue behaviors of two biomedical Mg alloys—AZ91D and WE43—in simulated body fluid. Acta Biomater. 2010;6:4605–13.
2. Cawley J, Metcalf JEP, Jones AH, Band TJ, Skupien DS. A tribological study of cobalt chromium molybdenum alloys used in metal-on-metal resurfacing hip arthroplasty. Wear. 2003;255:999–1006.
3. Morais S, Pereira MC. Application of stripping voltammetry and microelectrodes in vitro biocompatibility and in vivo toxicity tests of AISI 316L corrosion products. J Trace Elem Med Biol. 2000;14:48–54.
4. Reclaru L, Ziegenhagen R, Eschler PY, Blatter A, Lamaître J. Comparative corrosion study of Ni-free austenitic stainless steels in view of medical applications. Acta Biomater. 2006;2:433–44.
5. Karimi S, Nickchi T, Alfantazi AM. Long-term corrosion investigation of AISI 316L, Co–28Cr–6Mo, and Ti–6Al–4V alloys in simulated body solutions. Appl Surf Sci. 2012;258:6087–96.
6. Cieslik M, Engvall K, Pan J, Kotarba A. Silane–parylene coating for improving corrosion resistance of stainless steel 316L implant material. Corr Sci. 2011;53:296–301.
7. Puchi-Cabrera ES, Staia MH, Ochoa-Pérez EA, Teer DG, Santana-Méndez YY, La Barbera-Rosa JG, Chicot D, Lesage J. Fatigue behavior of a 316L stainless steel coated with a DLC film deposited by PVD magnetron sputter ion plating. Mater Sci Eng A. 2010;527:498–508.
8. Braic M, Balanceau M, Braic V, Vladescu A, Pavelescu G, Albulescu M. Synthesis and characterization of TiN, TiAlN and TiN/TiAlN biocompatible coatings. Surf Coat Technol. 2005;200:1014–7.
9. Wang L, Su JF, Nie X. Corrosion and tribological properties and impact fatigue behavior of TiN- and DLC-coated stainless steel in a simulated body fluid environment. Surf Coat Technol. 2010;205:1599–605.
10. Antunes RA, Rodas ACD, Lima NB, Higa OZ, Costa I. Study of the corrosion resistance and in vitro biocompatibility of PVD TiCN-coated AISI 316L austenitic stainless steel for orthopedic applications. Surf Coat Technol. 2010;205:2074–81.
11. Roman D, Bernardi J, Amorim CLG, Souza FS, Spinelli A, Giacomelli C, Figueroa CA, Beaumvol IJR, Basso RLO. Effect of deposition temperature on microstructure and corrosion resistance of ZrN thin films deposited by DC reactive magnetron sputtering. Mater Chem Phys. 2011;130:147–53.
12. Dorner-Reisel A, Schürer C, Irmer G, Müller E. Electrochemical corrosion behaviour of uncoated and DLC coated medical grade Co28Cr6Mo. Surf Coat Technol. 2004;177–178:830–7.

13. Krishnan LK, Varghese N, Muraleedharan CV, Bhuvaneshwar GS, Derangere F, Sampeur Y, Suryanarayanan R. Quantitation of platelet adhesion to Ti and DLC-coated Ti in vitro using ^{125}I-labeled platelets. Biomol Eng. 2002;19:251–3.
14. Dearnaley G, Arps JH. Biomedical applications of diamond-like carbon (DLC) coatings: a review. Surf Coat Technol. 2005;200: 2518–24.
15. Morshed MM, Cameron DC, McNamara BP, Hashmi MSJ. Pretreatment of substrates for improved adhesion of diamond-like carbon films on surgically implantable metals deposited by saddle field neutral beam source. Surf Coat Technol. 2003;174–175:579–83.
16. Takeno T, Sugawara T, Miki H, Takagi T. Deposition of DLC film with adhesive W-DLC layer on stainless steel and its tribological properties. Diam Relat Mater. 2009;18:1023–7.
17. Bewilogua K, Cooper CV, Specht C, Schröder J, Wittorf R, Grishke M. Effect of target material on deposition and properties of metal-containing DLC (Me-DLC) coatings. Surf Coat Technol. 2000;127:224–32.
18. Wang DY, Chang YY, Chang CL, Huang YW. Deposition of diamond-like carbon films containing metal elements on biomedical Ti alloys. Surf Coat Technol. 2005;200:2175–80.
19. Baba K, Hatada R. Deposition and characterization of Ti- and W-containing diamond-like carbon films by plasma source ion implantation. Surf Coat Technol. 2003;169–170:287–90.
20. Corbella C, Pascual E, Canillas A, Bertran E, Andújar JL. Visible and infrared ellipsometry applied to the study of metal-containing diamond-like carbon coatings. Thin Solid Films. 2004;455–456: 370–5.
21. Moura e Silva CW, Branco JRT, Cavaleiro A. How can H content influence the tribological behaviour of W-containing DLC coatings. Solid State Sci. 2009;11:1778–82.
22. Mansano RD, Ruas R, Mousinho AP, Zambom LS, Pinto TJA, Amoedo LH, Massi M. Use of diamond-like carbon with tungsten (W-DLC) films as biocompatible material. Surf Coat Technol. 2008;202:2813–6.
23. Cliff JB, Kreuzec HW, Ehrhardt CJ, Wunschel DS. Chemical and physical signatures for microbial forensics. 1st ed. London: Humana Press; 2012.
24. Lowe T, Chen Q, Fernando Q, Keith R, Gandolfi AJ. Elemental analysis of renal slices by proton-induced X-ray emission. Environ Health Perspect. 1993;101:302–8.
25. Williams ET. Applications of particle-induced X-ray emission to research in biology and medicine. Biol Trace Elem Res. 1987;12: 19–31.
26. Jallot E, Raissle O, Soulie J, Lao J, Guibert G, Nedelec JM. Quantitative chemical mapping of relevant trace elements at biomaterials/biological media interfaces by ion beam methods. Adv Eng Mat. 2010;12:B245–55.
27. Guibert G, Irigaray JL, Moretto Ph, Sauvage T, Kemeny JL, Cazenave A, Jallot E. Characterisation by PIXE-RBS of metallic contamination of tissues surrounding a metallic prosthesis on a knee. Nucl Instrum Methods B. 2006;251:246–56.
28. Barbotteau Y, Irigaray JL, Moretto Ph. PIXE characterization of tissues surrounding metallic prostheses coated with biological glasses. Nucl Instrum Methods B. 2004;215:214–22.
29. Ektessabi AM, Hamdi M. Characterization of calcium phosphate bioceramic films using ion beam analysis techniques. Surf Coat Technol. 2002;153:10–5.
30. Lao J, Nedelec JM, Moretto Ph, Jallot E. Micro-PIXE-RBS methods highlighting the influence of phosphorus on the in vitro bioactivity of sol-gel derived glass particles in the SiO_2–CaO–P_2O_5 system. Nucl Instrum Methods B. 2008;266:2412–7.
31. Oudadesse H, Irigaray JL, Barbotteau Y, Brun V, Moretto Ph. Combined PIXE and SEM study of the behaviour of trace elements in gel formed around implant coated with bioactive glass. Nucl Instrum Methods B. 2002;190:458–65.
32. Ahn SH, Choi YS, Kim JG, Han JG. A study on corrosion resistance characteristics of PVD Cr–N coated steels by electrochemical method. Surf Coat Technol. 2002;150:319–26.
33. Elsener B, Rota A, Böhni H. Impedance study on the corrosion of PVD and CVD titanium nitride coatings. Mater Sci Forum. 1989;44–45:29–38.
34. Weng D, Jokiel P, Uebleis A, Boehni H. Corrosion and protection characteristics of zinc and manganese phosphate coatings. Surf Coat Technol. 1996;88:147–56.
35. Liu C, Bi Q, Leyland A, Matthews A. An electrochemical impedance spectroscopy study of the corrosion behaviour of PVD coated steels in 0.5 N NaCl aqueous solution. Part II: EIS interpretation of corrosion behaviour. Corr Sci. 2003;45:1257–73.
36. Merl DK, Panjan P, Cekada M, Macek M. The corrosion behavior of Cr-(C, N) PVD hard coatings deposited on various substrates. Electrochim Acta. 2004;49:1527–33.
37. Aburaya JH, Added N, Tabacniks MH, Rizzutto MA, Barbosa MDL. X-ray production yield in standardized thick target PIXE. Nucl Instrum Methods B. 2006;249:792–5.
38. Saiki M, Rogero SO, Costa I, Correa OV, Higa OZ. Characterization of ear piercing studs and their corrosion products by neutron activation analysis. J Radioanal Nucl Chem. 2001;248: 133–6.
39. International Organization for Standardization, ISO 10993-5. Biological testing of medical and dental materials devices—part 5. Switzerland: Tests for cytotoxicity: in vitro methods; 1992.
40. Prawer S, Nugent KW, Lifshitz Y, Lempert GD, Grossman E, Kulik J, Avigal I, Kalish R. Systematic variation of the Raman spectra of DLC films as a function of sp^2:sp^3 composition. Diam Relat Mater. 1996;5:433–8.
41. Choudbury S, Laugier MT, Ralman IZ. Characterization of DLC coatings deposited by rf magnetron sputtering. J Mater Proc Technol. 2004;153–154:804–10.
42. Ferrari AC, Robertson J. Interpretation of Raman spectra of disordered and amorphous carbon. Phys Rev B. 2000;61: 14095–107.
43. Liu H, Xu Q, Wang C, Zhang X, Tang B. Investigating the microstructure and mechanical behaviors of DLC films on AISI52100 bearing steel surface fabricated by plasma immersion ion implantation and deposition. Surf Coat Technol. doi: 10.1016/j.surfcoat.2012.06.071.
44. Li Y, Qu L, Wang F. The electrochemical corrosion behavior of TiN and (Ti, Al)N coatings in acid and salt solution. Corr Sci. 2003;45:1367–81.
45. Panjan P, Cekada M, Panjan M, Merl DK. Growth defects in PVD hard coatings. Vacuum. 2010;84:209–14.
46. Kim HG, Ahn SH, Kim JG, Park SJ, Lee KR. Electrochemical behavior of diamond-like carbon films for biomedical applications. Thin Solid Films. 2005;475:291–7.
47. Choi HW, Lee KR, Park SJ, Wang R, Kim JG, Oh KH. Effects of plastic strain of diamond-like carbon coated stainless steel on the corrosion behavior in simulated body fluid environment. Surf Coat Technol. 2008;202:2632–7.
48. Chenglong L, Dazhi Y, Guoqiang L, Min Q. Corrosion resistance and hemocompatibility of multilayered Ti–TiN–coated surgical AISI 316L stainless steel. Mater Lett. 2005;59:3813–9.
49. Pérez FJ, Hierro MP, Gómez C, Martínez L, Viguri PG. Ion implantation as a surface modification technique to improve localised corrosion of different stainless steels. Surf Coat Technol. 2002;155:250–9.
50. Kissi M, Bouklah M, Hammouti B, Benkaddour M. Establishment of equivalent circuits from electrochemical impedance spectroscopy study of corrosion inhibition of steel by pyrazine in sulphuric acidic solution. Appl Surf Sci. 2006;252:4190–7.
51. Boukamp BA. A package for impedance/admittance data analysis. Solid State Ion. 1986;18–19:136–40.

52. Abouzari MRS, Berkemeier F, Schmitz G, Wilmer D. On the physical interpretation of constant phase elements. Solid State Ion. 2009;180:922–7.
53. Assis SL, Wolynec S, Costa I. Corrosion characterization of titanium alloys by electrochemical techniques. Electrochim Acta. 2006;51:1815–9.
54. Zou JX, Zhang KM, Hao SZ, Dong C, Grosdidier T. Mechanisms of hardening, wear and corrosion improvement of 316L stainless steel by low energy high current pulsed electron beam surface treatment. Thin Solid Films. 2010;519:1404–15.
55. Kocijan A, Merl DK, Jenko M. The corrosion behaviour of austenitic and duplex stainless steels in artificial saliva with the addition of fluoride. Corr Sci. 2011;53:776–83.
56. Ge HH, Zhou GD, Wu WQ. Passivation model of 316 stainless steel in simulated cooling water and the effect of sulfide on the passive film. Appl Surf Sci. 2003;211:321–34.
57. Yoo YH, Hong JH, Kim JG, Lee HY, Han JG. Effect of Si addition to CrN coatings on the corrosion resistance of CrN/stainless steel coating/substrate system in a deaerated 3.5 wt% NaCl solution. Surf Coat Technol. 2007;201:9518–23.
58. Li L, Niu E, Lv G, Zhang X, Chen H, Fan S, Liu C, Yang SZ. Synthesis and electrochemical characteristics of Ta–N thin films fabricated by cathodic arc deposition. Appl Surf Sci. 2007;253:6811–6.
59. Grips VKW, Selvi VE, Barshilia HC, Rajam KS. Effect of electroless nickel interlayer on the electrochemical behavior of single layer CrN, TiN, TiAlN coatings and nanolayered TiAlN/CrN multilayer coatings prepared by reactive dc magnetron sputtering. Electrochim Acta. 2006;51:3461–8.
60. Hang R, Ma S, Chu PK. Corrosion behavior of DLC-coated NiTi alloy in the presence of serum proteins. Diam Relat Mater. 2010;19:1230–4.
61. Sharma R, Barhai PK, Kumari N. Corrosion resistant behaviour of DLC films. Thin Solid Films. 2008;516:5397–403.
62. Mohan L, Anandan C, Grips VKW. Corrosion behavior of titanium alloy beta-21S coated with diamond like carbon in Hank's solution. Appl Surf Sci. 2012;258:6331–40.
63. Marin E, Guzman L, Lanzutti A, Fedrizzi L, Saikkonen M. Chemical and electrochemical characterization of hybrid PVD + ALD hard coatings on tool steel. Electrochem Commun. 2009;11:2060–3.
64. Korhonen AS. Corrosion of thin hard PVD coatings. Vacuum. 1994;45:1031–4.
65. Egeni GP, Jaksic M, Moschini G, Passi P, Piatelli A, Rossi P, Rudello V, Tauro L. PIXE and micro-PIXE studies of ion release around endosseous implants in animals. Nucl Instrum Methods Phys Res B. 1996;109/110:289–93.
66. Olivares R, Rodil SE, Arzate H. Osteoinduction properties of graphite-like amorphous carbon films evaluated in vitro. Diam Relat Mater. 2007;16:1858–67.
67. Cui FZ, Qing XL, Lib DJ, Zhao J. Biomedical investigations on CN_x coating. Surf Coat Technol. 2005;200:1009–13.
68. Vaid C, Murugavel S. Alkali oxide containing mesoporous bioactive glasses: Synthesis, characterization and in vitro bioactivity. Mater Sci Eng C. 2013;33:959–68.
69. Hollstein F, Louda P. Biocompatible low reflective coatings for surgical tools using reactive d.c.-magnetron sputtering and arc evaporation: a comparison regarding steam sterilization resistance and nickel diffusion. Surf Coat Technol. 1999;120–121:672–81.
70. Salgueiredo E, Vila M, Silva MA, Lopes MA, Santos JD, Costa FM, Silva RF, Gomes PS, Fernandes MH. Diam Relat Mater. 2008;17:878–81.
71. Sui JH, Gao ZY, Cai W, Zhang ZG. DLC films fabricated by plasma immersion ion implantation and deposition on the NiTi alloys for improving their corrosion resistance and biocompatibility. Mater Sci Eng A. 2007;454–455:472–6.
72. Bendavid A, Martin PJ, Comte C, Preston EW, Haq AJ, Ismail FSM, Singh RK. The mechanical and biocompatibility properties of DLC-Si films prepared by pulsed DC plasma activated chemical vapor deposition. Diam Relat Mater. 2007;16:1616–22.
73. Witten ML, Sheppard PR, Witten BL. Tungsten toxicity. Chem Biol Interact. 2012;196:87–8.